OPEN

Bone Mineral Density Estimations From Routine Multidetector Computed Tomography: A Comparative Study of Contrast and Calibration Effects

Johannes Kaesmacher, MD, Hans Liebl, MD,† Thomas Baum, MD,‡ and Jan Stefan Kirschke, MD**

Introduction: Phantom-based (synchronous and asynchronous) and phantomless (internal tissue calibration based) assessment of bone mineral density (BMD) in routine MDCT (multidetector computed tomography) examinations potentially allows for diagnosis of osteoporosis. Although recent studies investigated the effects of contrast-medium application on phantom-calibrated BMD measurements, it remains uncertain to what extent internal tissue-calibrated BMD measurements are also susceptible to contrast-medium associated density variation. The present study is the first to systemically evaluate BMD variations related to contrast application comparing different calibration techniques.

Purpose: To compare predicative performance of different calibration techniques for BMD measurements obtained from triphasic contrast-enhanced MDCT.

Materials and Methods: Bone mineral density was measured on nonenhanced (NE), arterial (AR) and portal-venous (PV) contrast phase MDCT images of 46 patients using synchronous (SYNC) and asynchronous (ASYNC) phantom calibration as well as internal calibration (IC). Quantitative computed tomography (QCT) served as criterion standard. Density variations were analyzed for each contrast phase and calibration technique, and respective linear fitting was performed.

Results: Both asynchronous calibration-derived BMD values (NE-ASYNC) and values estimated using IC (NE-IC) on NE MDCT images did reasonably well in predicting QCT BMD (root-mean-square deviation, 8.0% and 7.8%, respectively). Average NE-IC BMD was 2.7% lower when compared with QCT ($P = 0.017$), whereas no difference could be found for NE-ASYNC ($P = 0.957$). All average BMD estimates derived from contrast-enhanced scans differed significantly from QCT BMD (all $P < 0.005$) and led to notable systemic BMD biases (mean difference at least > 6.0 mg/mL). All regression fits revealed a consistent linear dependency (R^2 range, 0.861–0.963). Overall accuracy and goodness of fit tended to decrease from AR to PV contrast phase. Highest precision and best linear fit could be reached using a synchronously scanned phantom (root-mean-square deviation, 9.4% for AR and 14.4% for PV). Both ASYNC and IC estimations performed comparably accurate and precise.

Conclusions: Our data suggest that internal calibration driven BMD measurements derived from contrast-enhanced MDCT need the same amount of post hoc contrast-effect adjustment as measurements using phantom calibration. Adjustment using linear correction equations can correct for systematic bias of bone density variations related to contrast application, irrespective of the calibration technique used.

Key Words: bone mineral density, phantom, internal calibration, MDCT, calibration, contrast medium, contrast agent

(*J Comput Assist Tomogr* 2017;41: 217–223)

Osteoporosis is the most prevalent bone disorder affecting our ageing societies and is characterized by a disruption of the delicate balance between bone resorption and bone formation.[1] Subsequent bone substance loss and changes in bone microarchitecture markedly favor the occurrence of fractures, which are associated with high morbidity and mortality.[1–4]

Computed tomography (CT)–derived assessment of bone mineral density (BMD) has evolved as a reliable alternative in the diagnosis of patients suffering from age-related bone loss.[5–7] The modality inherits a variety of advantages compared with dual-energy X-ray absorptiometry (DXA),[8,9] the modality currently implemented in the World Health Organization definition of osteoporosis.[10] Because many patients undergo abdominal multidetector CT (MDCT) for clinical reasons, routine MDCT-derived measurements may lead to a redundancy of additional quantitative CT (QCT) scans and thus minimize radiation exposure and health care costs. In particular, cancer patients may benefit from this approach, because they usually undergo multiple MDCT examination while concomitantly being exposed to an increased risk of bone loss due to cancer related treatment,[11] paraneoplastic effects, and due to the advanced mean age of this patient population.

There are 2 major methods in calculating MDCT-derived BMD: phantomless and phantom-based estimations. When using a calibration phantom, reference values can be obtained from each individual scan by measuring the reference regions of the simultaneously scanned calibration phantom (synchronous [SYNC]), alternatively a larger number of phantom measurements from different scans can be averaged (asynchronous [ASYNC]).

In contrast to phantom calibration, phantomless measurements utilize tissues other than bone from the same image as an internal calibration reference (IC). Both methods have shown to result in reliable measurements and to be highly reproducible.[12–14] The phantomless method introduced by Mueller et al[13] uses muscle and fat tissue as internal reference. Although such methods may be confounded by heterogeneous Hounsfield unit (HU) distribution within the muscle as well as its dependency on the respective hydration and physical activity state of a patient,[15] this method provides unprecedented opportunities utilizing clinical routine abdominal CT, which where run without a designated osteodensitometry phantom.[16]

Several recent studies draw attention to the feasibility of contrast-enhanced CTs for BMD calculation.[17–19] Most studies use phantom-based density measurements and propose linear conversion equations yielding high reliability[17] and allowing

From the *Department of Diagnostic and Interventional Neuroradiology, Klinikum rechts der Isar, Technical University Munich, Munich; †Department of Radiology and Neuroradiology, Evangelisches Krankenhaus Oldenburg, Oldenburg; and ‡Department of Diagnostic and Interventional Radiology, Klinikum rechts der Isar, Technical University Munich, Munich, Germany.

Received for publication May 9, 2016; accepted August 15, 2016.

Correspondence to: Johannes Kaesmacher, MD, Department of Diagnostic and Interventional Neuroradiology Klinikum rechts der Isar, Technical University Munich Ismaninger Str. 22 81675 Munich, Germany (e-mail: j.kaesmacher@tum.de).

Johannes Kaesmacher and Hans Liebl contributed equally.

This work was supported by grants of the Deutsche Forschungsgemeinschaft (DFG BA 4085/2-1 and BA 4906/1-1) and by grants of the European Research Council (ERC-StG-2014 iBack 637164).

The authors declare no conflict of interest.

DOI: 10.1097/RCT.0000000000000518

reasonably accurate clinical stratification.[20] However, if designated reference phantoms are omitted and tissue of the patient is used as an internal reference for calibration, the variable uptake of contrast-agent, owing to the specific tissue properties and composition, results in new challenges. Hence, it remains unclear to which extent BMD measurements based on phantomless, internal tissue-based calibration is susceptible to density variation related to contrast agent application.

This study is the first to investigate density offsets associated with contrast medium application and to propose corresponding correction equations for both, phantom-calibrated BMD measurements (synchronous and asynchronous) and a phantomless BMD measurement method[13] using triphasic contrast-enhanced MDCT images.

METHODS

This retrospective study was conducted with approval of the institutional ethical review board (5022/11). The study was in accordance with the ethical standards of the 1964 Declaration of Helsinki and its later amendments.[21]

Study Subjects

All spine images were derived from our digital picture archiving communication system (PACS) (Sectra AB, Linkoeping, Sweden). Images acquired over the course of 3 years (January 1, 2010, and December 1, 2013) were included into further analysis if the following criteria were met: (1) abdominal MDCT scan (dedicated to investigate liver or kidney pathologies); (2) precontrast images as well as standardized biphasic contrast protocol with 5-mm axial reformations, 3-mm sagittal reformations; and (3) intact morphology of the lumbar region L1–L3. All patients with orthopedic hardware or presence of beam hardening artifacts were excluded; further exclusion criteria consisted of: presence of pathological bone changes other than osteoporosis, such as fracture, osseous metastasis, circumscribed sclerosis (eg, bone island), circumscribed lucencies (eg, cystic lesions), vascular malformations, hemangiomas, known hematological disorders, or severe degeneration.

Imaging

Routine abdominal contrast-enhanced MDCT scans were performed with 2 scanners used at our institution: a whole-body 256-row MDCT scanner (iCT; Philips Medical Care, Best, The Netherlands) with a dedicated calibration phantom (Mindways Osteoporosis Phantom, San Francisco, Calif) placed in the scanner mat beneath the functional spinal segment units and a 64-row MDCT scanner (Somatom Sensation Cardiac 64; Siemens Medical Solutions, Erlangen, Germany) with a calibration phantom (Osteo Phantom; Siemens Medical Solutions) were used. All routine abdominal contrast-enhanced MDCT images were obtained following the same standard protocol on both scanners. Scanning parameters were 120-kVp tube voltage, an adapted average effective tube current of 200 mAs, and minimum collimation (0.6 mm). Precontrast images were acquired, and delayed scans were performed after standardized administration of intravenous contrast medium (Imeron 400; Bracco, Konstanz, Germany) using a high-pressure injector (Fresenius Pilot C; Fresenius Kabi, Bad Homburg, Germany). Intravenous contrast agent injection was performed with a flow rate of 3 mL/s, and a body weight–dependent dose (80 mL for body weight up to 80 kg, 90 mL for body weight up to 100 kg, and 100 mL for body weight over 100 kg). Acquisition of the arterial (AR) contrast phase images was automatically triggered after a threshold of contrast agent concentration was exceeded within a region of interest (ROI) placed at the aorta. Portal-venous (PV) contrast-phase images were acquired with a standard delay of 70 seconds.

Image Analysis

All standard abdominal images and additional sagittal reformations were loaded into the institutional PACS, and circular ROIs were manually placed by a radiologist in the reference fields of the calibration phantoms in the axial images as well as in the midsectional trabecular parts of each lumbar vertebral body L1–L3 in the axial plane while ensuring equidistant placement to both endplates using the sagittal reformation as a reference. Values were calculated using the density measurement tool of the PACS software as described before.[20] The ROI diameter was standardized to 50% of the superior-inferior vertebral body dimension. Regions of interest were created in the ventral halves of the trabecular compartments of the vertebral bodies to avoid contrast enhancement of the posterior vertebral venous plexus, thus determining trabecular attenuation of L1–L3 (in HU) for each contrast-phase image set separately, as described earlier (see Fig. 1).[19] Attenuation values were then converted into QCT equivalent BMD values (in milligrams of calcium hydroxylapatite per milliliter) using the reference measurements obtained from the according calibration phantom in the same scan (SYNC) or the average obtained from all phantom scans (ASYNC). The BMD values using the Phillips BMD option were calculated according to manufacturer's recommendation and as described earlier.[13] In short, a 9-mm-high cylinder volume of interest (VOI) (see Fig. 2, VOI with grey border and squares, annotation: Organ = L1) was

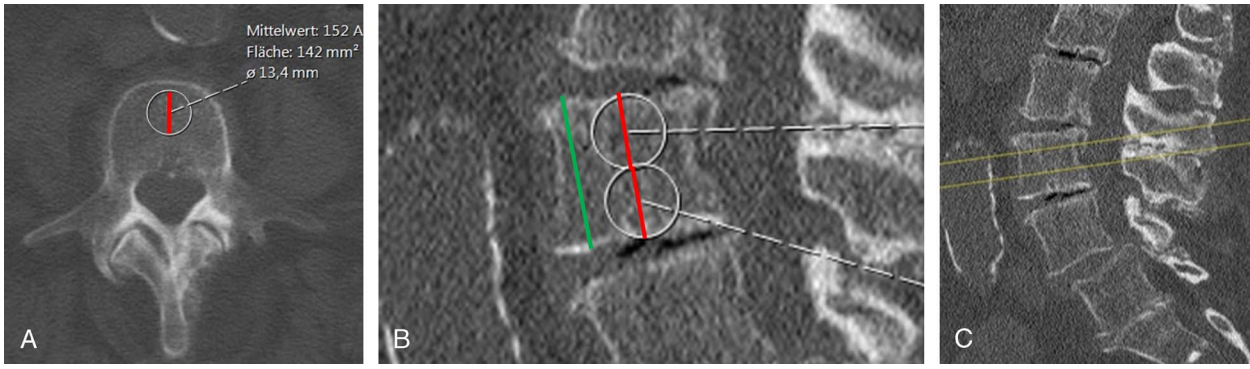

FIGURE 1. Measurement of attenuation values. A, Measurement ROI (white border, diameter in black) for calculation attenuation values in the anterior part of the vertebral body using axial 10 mm average intensity projections. B, The ROI in A was standardized to one half of the superior-inferior vertebral body dimensions. C, Axial slices for measurement were ensured to be in equidistant localization to the inferior and superior endplates using a sagittal reformation as a reference.

automatically placed into the trabecular compartment of each vertebra (L1–L3) and 2 additional ROIs were manually placed at the midsectional level of each respective vertebra: 1 in the paraspinal muscle (Fig. 2, ROI with black border, annotation: Organ = Muscle) and 1 in the subcutaneous fat (Fig. 2, ROI with white border, annotation: Organ = Fat). A random sample of 10 subjects was chosen and reanalyzed by the same investigator to calculate the reproducibility error.

Statistical Analysis

All statistical analyses were performed using SPSS (V.23.0; IBM Corporation, Armonk, NY). The Kolmogorov-Smirnov analysis exhibited no significant difference from a normal distribution ($P > 0.1$). Precision errors were calculated using root-mean-square averages of the coefficients of variation (CV) of repeated measurements.[22] The BMD estimates of different techniques and based on different contrast phase scans were directly compared with QCT values using root-mean-square deviation and respective CVs. A prior correction was not used; instead, the results of this comparison indicate how a correction can be applied for further studies. Mean errors and 95% confidential intervals were displayed using standard Bland-Altman plots. Correlations were displayed as Pearson correlation coefficient r. Mean BMDs were compared using paired samples *t* test. R^2 was used for estimating goodness of fit and compared using Fisher z transformation. All *P* values were 2-sided.

RESULTS

Study Population and BMD Estimation on Native Images

The final study population included 46 patients (mean age: 64.2 ± 12.8 years; 32.7% female), with a mean QCT BMD of 123.5 ± 40.0 mg/mL. There was an inverse correlation between age and BMD ($r = -0.515$; $P < 0.001$). Both asynchronous calibration–derived BMD values (NE-ASYNC) and values estimated using IC (NE-IC) on NE MDCT images did reasonably well in predicting QCT BMD (see Table 1 for corresponding CVs). Values did not differ significantly between QCT and NE-ASYNC (123.5 vs 123.4 mg/mL; $P = 0.957$) and linear regression revealed a near optimal fit (QCT BMD = 4.6 mg/mL + 0.96 × NE-ASYNC; $R^2 = 0.939$; see Fig. 3). The NE-IC tended to underestimate QCT-derived BMD (mean difference, 3.3 mg/mL), and the average BMD was 2.7% lower ($P = 0.017$), accordingly. However, applying a linear regression model revealed a comparably precise fit (QCT BMD = 3.36 mg/mL + 1 × NE-IC; $R^2 = 0.947$).

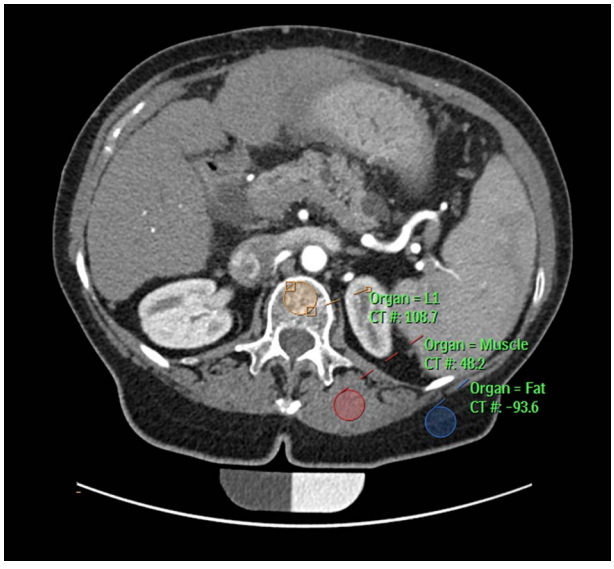

FIGURE 2. Snapshot of using the Philips BMD options. Automatic placement of the vertebral volume of interest (orange) and manual placement of the ROIs of the paraspinal muscle (red) and fat tissue (blue).

Contrast Effect for Different BMD Estimation Methods

All average BMD estimates derived from contrast-enhanced scans differed significantly from QCT BMD (all $P < 0.005$). Irrespective of the applied calculation method, contrast administration led to notable BMD offsets (see Table 1 and Fig. 4 for respective mean differences). Phantom-based (synchronous) derived BMDs were approximately 9% higher for AR (132.2 vs 123.5 mg/mL) and approximately 13% higher for PV (139.4 vs 123.5 mg/mL) compared with QCT BMD values. Also, BMD estimates using asynchronous phantom calibration were higher in the contrast-enhanced scans as compared with QCT BMD (AR, 132.0 vs 123.5 mg/mL; ~7% PV: 139.3 vs 123.5 mg/mL; ~13%). The internal calibration method, as applied to contrast-enhanced scans, yielded approximately 5% (AR, 129.5 vs 123.5 mg/mL)/ 9% (PV, 134.5 vs 123.5 mg/mL) higher BMD values as opposed to the mean reference value (QCT).

Subsequently, offsets were generally smaller in the IC BMD estimates (AR, −11.0 vs −13.9 vs −15.8 mg/mL; PV: −6.0 vs −8.7 vs −8.6 mg/mL for IC, SYNC, and ASYNC, respectively). Note, however, that NE-IC BMDs were associated with a systemic underestimation of QCT BMD (ie, a contrast-effect opposing trend: positive offset of 3.3 mg/mL when compared with QCT, see above). The PV imaging was generally associated with more severe density changes as compared with AR imaging (mean difference AR for all techniques: 7.8 mg/mL; mean difference PV for all techniques: 14.3 mg/mL; see respective single technique mean differences in Table 1 and Fig. 4).

All regression fits revealed a coherent linear dependency (R^2 range, 0.861–0.963; see Fig. 3). However, overall accuracy and, albeit less pronounced, linear fit for all methods tended to decrease from AR to PV CT (compare consistently lower CVs for PV vs AR scans, see Table 1). Highest precision and best linear fit could be reached using a synchronously scanned phantom. Accuracy was comparable for both synchronous and asynchronous phantom-based calibration methods. However, both synchronous and asynchronous phantom calibration, as applied to contrast-enhanced scans, yielded better linear fits when compared with the internal reference approach ($R^2 = 0.963$ vs 0.923 vs 0.881 and 0.962 vs 0.904 vs 0.861 for AR-SYNC vs AR-ASYNC vs AR-IC and PV-SYNC vs PV-ASYNC vs PV-IC, respectively). This reached statistical significance only for synchronous phantom calibration as opposed to internal tissue reference method only ($P < 0.05$; Fisher *z* transformation).

A trend for an age dependency, resulting in higher changes in BMD in younger subjects, was observed when comparing NE and AR BMDs ($r = -0.275$; $P = 0.064$) as well as NE and PV BMDs ($r = -0.239$, $P = 0.110$), when using phantom-based models. This effect was not observable when using the internal tissue calibration technique (AR phase: $r = 0.097$, $P = 0.523$; PV phase: $r = -0.093$; $P = 0.540$).

Reproducibility

The reproducibility errors, calculated as the root mean square of the single CV for the lumbar BMD measurements in sagittal

TABLE 1. Accuracy Comparison of Different BMD Estimation Techniques

	SYNC		ASYNC			IC		
	AR	PV	NE	AR	PV	NE	AR	PV
RMSD, mg/mL	11.57	17.72	9.86	13.99	19.98	9.67	14.98	18.48
CV(RMSD) [%]	9.4%	14.4%	8.0%	11.3%	16.2%	7.8%	12.1%	15.0%
Mean difference to QCT BMD, mg/mL	−8.7	−15.9	0.1	−8.6	−15.8	3.3	−6.0	−11.3

RMSD indicates root-mean-square deviation.

reformations were 5.6%, 3.5%, and 3.1% for NE, AR and PV in the phantom-based BMD calculations; errors were 5.1%, 3.2%, and 3.3% for NE, AR, and PV in the asynchronous calibration and 8.2%, 8.8%, and 6.6% for NE, AR, and PV in the internal tissue calibrations.

DISCUSSION

The present study demonstrates that contrast-medium associated systematic biases in BMD measurements based on routine MDCT images are equally present when using phantomless, internal tissue calibration techniques as well as phantom-based calibration methods. Although the present study concurs with current concepts of simple linear correcting equations in phantom-based adjustment of contrast media-associated density alterations, it also suggests the same need for an adequate correction method in BMD estimates obtained from MDCT scans, which were run without a phantom. The data support a rational for calculating BMD on contrast-enhanced CT scans using either asynchronous phantom calibration or the internal calibration method proposed by Mueller et al[13] and by further applying respective additional correction equations as defined in the present study (see Fig. 3).

Bauer et al[18] and Baum et al[19] derived BMD conversion equations from routine abdominal MDCT scans. They were able to

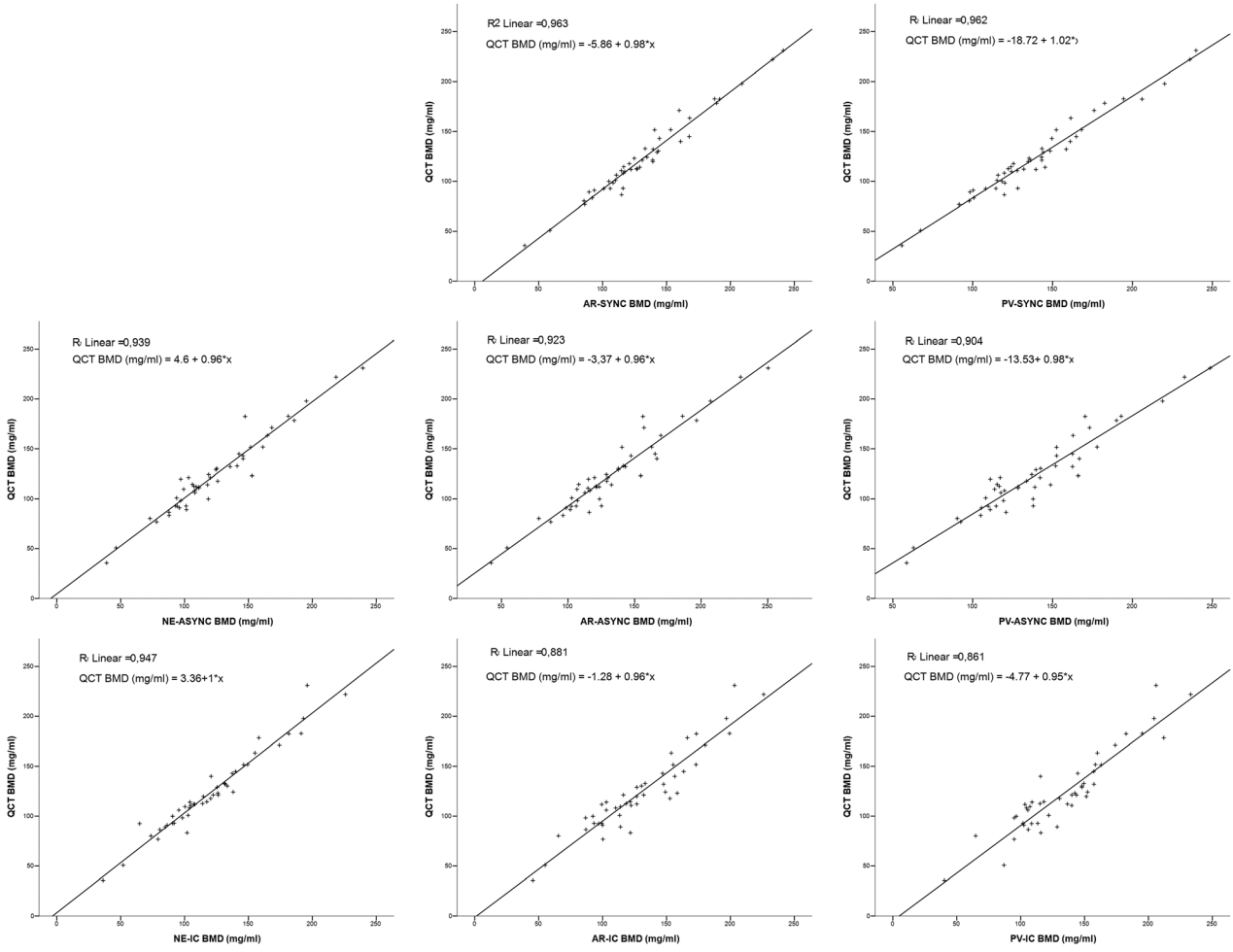

FIGURE 3. Linear regressions for different BMD estimation techniques in triphasic MDCT. Upper row, synchronous phantom calibration method; mid row, asynchronous phantom calibration method; lower row, internal calibration method; left column, nonenhanced CT scans; mid column, arterial-phase CT scans; right column portal phase CT scans.

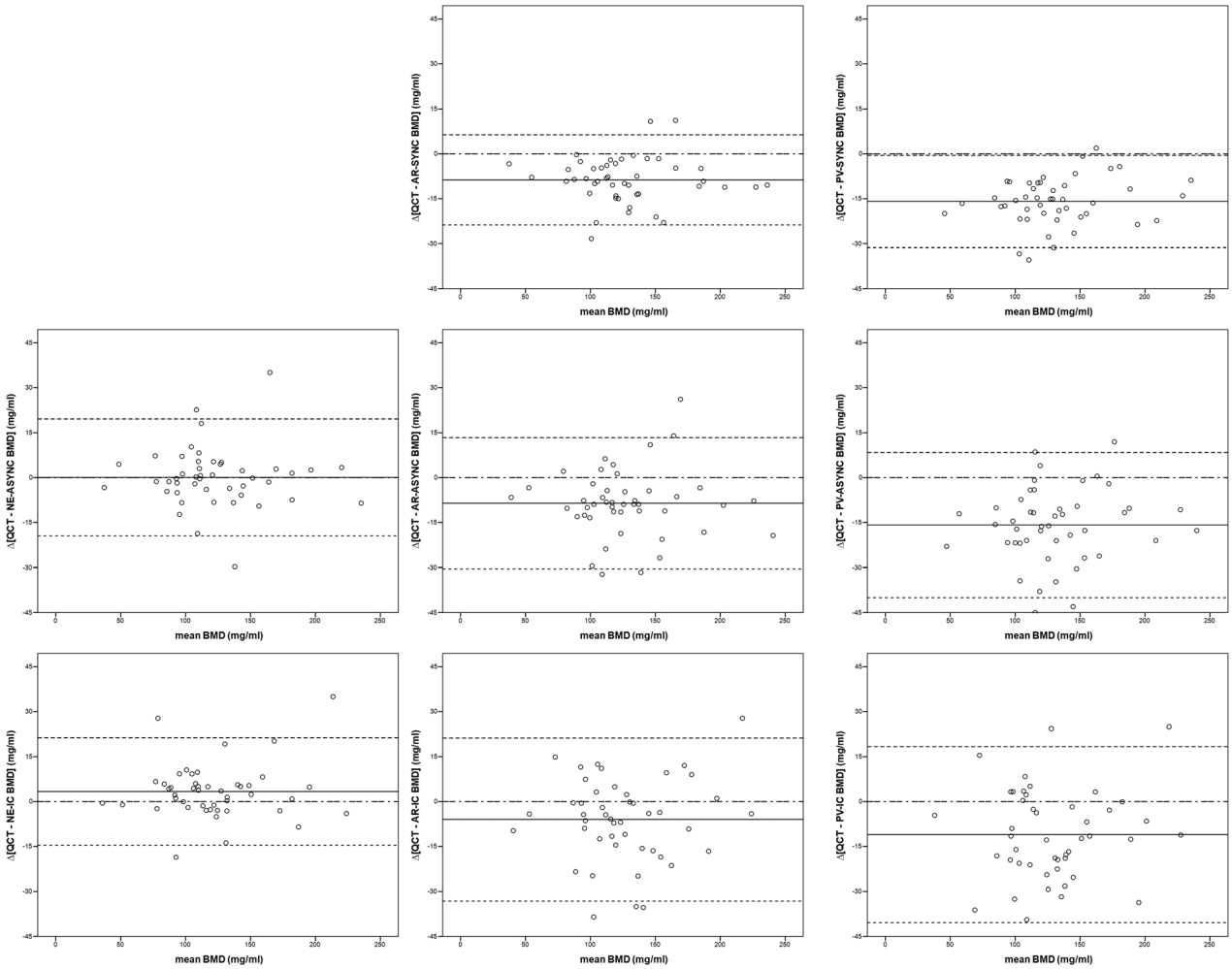

FIGURE 4. Bland-Altman plots for different BMD estimation techniques in triphasic MDCT. Upper row, synchronous phantom calibration method; mid row, asynchronous phantom calibration method; lower row, internal calibration method; left column, nonenhanced CT scans; mid column, arterial-phase CT scans; right column portal phase CT scans.

show that this methods yields potential for both clinical fracture status stratification[19] as well as prediction of incidental osteoportic vertebral fractures.[20] However, their measurements were limited to MDCT with PV contrast phase scans only and required a phantom in the table mat. In contrast, Acu et al[23] investigated the time and age dependency of BMD estimation from MDCT scans with intravenous contrast agent administration without requiring a reference phantom. In contrast to the internal calibration method, evaluated in this study, they used previously published conversion factors for HU-to-BMD conversion. Mueller and colleagues[13] performed internal tissue-based calibration using patients muscle and fat tissue as reference regions and only included a total of 3 AR phase and 6 PV phase scans. However, owing to the limited sample size receiving contrast agent, they did not systemically analyze the effect of contrast-associated density alterations on BMD estimation regarding their published method.[13] Instead, they postulated that congenerous contrast medium effects were similar to phantom-calibrated scans and subsequently applied a previously published universal conversion formula for the contrast-enhanced scans.[18] Therefore, the present study is the first to systematically evaluate contrast effects in BMD measurements derived from MDCT imaging comparing phantom calibration (synchronous/asynchronous) as well as phantomless, internal tissue calibration. Hence, these data provide the first conclusive evidence demonstrating feasibility and respective correction equations.

The time-dependent pattern of contrast-medium associated density variations within the muscle and fat are not only highly individual but also inconsistent regarding the net trend.[24] The current data suggest that both the region to be measured and the regions to serve as internal reference are unequally affected by attenuation changes, and therefore additional adjustment methods are required. The methods intrinsic offsets (respecting systemic overestimation/underestimation on native CT images) were equal among all methods analyzed, and thus, one may conclude that intrinsic calibration do not significantly alter neither the need nor the extent of post hoc correction.

On the one hand, the proximal femur is more suited for BMD measurements from contrast-enhanced CT scans, because it is less susceptible for contrast medium–associated density alterations[18,25–27] and has been shown to correspond well with DXA-derived BMD values.[28] On the other hand, it was shown that spinal DXA measurement are more precise in predicting spinal fracture risk and vertebral fracture load than are DXA measurements at the femur, underlining the general need for measuring local BMD as close as possible to the area

where the fracture risk is to be predicted.[29–32] Thus, although more susceptible to contrast agent–associated effects, BMD measurements at the lumbar spine from contrast enhanced CT scans from clinical routine imaging may be warranted and add additional value to the patients' individual spine fracture risk evaluation. Further BMD values obtained from routine contrast-enhanced CT scans (ie, kidney, liver) do not routinely include the level of the femur and using BMD estimations at the level of the lumbar spine hence increases the number of clinical (contrast-enhanced) CT scans suitable for nondedicated BMD estimations.

Precision and accuracy are the two most referred to characteristics for description of any measurement system. Whereas precision reflects the closeness of agreement among different subsets of results, accuracy refers to the closeness of a measurement according to the true value. When referring to images acquired without a phantom, asynchronous phantom calibration yielded comparably accurate results as compared to the internal tissue calibration method. However, BMD values derived from asynchronous calibration on contrast-enhanced scans yielded better linear fits, and thus easier and more precise correction capacity, compared with BMD values derived from the internal tissue calibration approach. The BMD values derived from nonenhanced CT scans using the internal calibration methods tended to be lower compared with QCT measurements, which is a finding shared by the research group, which initially introduced the method.[13]

A major limitation arises due to the relatively small size of the study cohort. Furthermore, future studies need to validate the proposed correction equations for the internal tissue calibration method and evaluate its clinical reliability with respect to fracture status stratification, and predictive capability. The generalizability of our correction equations should be handled with caution, because they may be substantially influenced by the scanner used, mat height, and other scanning parameters.

CONCLUSIONS

Internal tissue–driven BMD estimations on contrast-enhanced scans are feasible and reasonably accurate and precise. The BMD measurements based on internal tissue calibration derived from contrast-enhanced MDCT imaging need similar contrast-effect adjustment as compared with measurements based on phantom calibration. Adjustment with simple linear regression is capable of evening out substantial systematic biases related to contrast medium application for BMD measurements, irrespective of the calibration technique used. Asynchronous phantom calibration yielded comparable accuracy and precision as did the phantomless calibration method and therefore should be considered as a viable option in BMD calculation based on contrast-enhanced MDCT.

REFERENCES

1. Nih Consensus Development Panel on Osteoporosis Prevention D, Therapy. Osteoporosis prevention, diagnosis, and therapy. *JAMA*. 2001; 285:785–795.
2. Boonen S, Autier P, Barette M, et al. Functional outcome and quality of life following hip fracture in elderly women: a prospective controlled study. *Osteoporos Int*. 2004;15:87–94.
3. Papaioannou A, Kennedy CC, Ioannidis G, et al. The impact of incident fractures on health-related quality of life: 5 years of data from the Canadian Multicentre Osteoporosis Study. *Osteoporos Int*. 2009;20: 703–714.
4. Ioannidis G, Papaioannou A, Hopman WM, et al. Relation between fractures and mortality: results from the Canadian Multicentre Osteoporosis Study. *CMAJ*. 2009;181:265–271.
5. Adams JE. Quantitative computed tomography. *Eur J Radiol*. 2009;71: 415–424.
6. Engelke K, Libanati C, Liu Y, et al. Quantitative computed tomography (QCT) of the forearm using general purpose spiral whole-body CT scanners: accuracy, precision and comparison with dual-energy X-ray absorptiometry (DXA). *Bone*. 2009;45:110–118.
7. Mao SS, Li D, Luo Y, et al. Application of quantitative computed tomography for assessment of trabecular bone mineral density, microarchitecture and mechanical property. *Clin Imaging*. 2015;40: 330–338.
8. Bolotin HH, Sievanen H, Grashuis JL, et al. Inaccuracies inherent in patient-specific dual-energy X-ray absorptiometry bone mineral density measurements: comprehensive phantom-based evaluation. *J Bone Miner Res*. 2001;16:417–426.
9. Antonacci MD, Hanson DS, Heggeness MH. Pitfalls in the measurement of bone mineral density by dual energy x-ray absorptiometry. *Spine (Phila Pa 1976)*. 1996;21:87–91.
10. Assessment of fracture risk and its application to screening for postmenopausal osteoporosis. Report of a WHO Study Group. *World Health Organ Tech Rep Ser*. 1994;843:1–129.
11. Smith MR, McGovern FJ, Fallon MA, et al. Low bone mineral density in hormone-naive men with prostate carcinoma. *Cancer*. 2001;91: 2238–2245.
12. Budoff MJ, Malpeso JM, Zeb I, et al. Measurement of phantomless thoracic bone mineral density on coronary artery calcium CT scans acquired with various CT scanner models. *Radiology*. 2013;267: 830–836.
13. Mueller DK, Kutscherenko A, Bartel H, et al. Phantom-less QCT BMD system as screening tool for osteoporosis without additional radiation. *Eur J Radiol*. 2011;79:375–381.
14. Budoff MJ, Khairallah W, Li D, et al. Trabecular bone mineral density measurement using thoracic and lumbar quantitative computed tomography. *Acad Radiol*. 2012;19:179–183.
15. Aubrey J, Esfandiari N, Baracos VE, et al. Measurement of skeletal muscle radiation attenuation and basis of its biological variation. *Acta Physiol (Oxf)*. 2014;210:489–497.
16. Aslam R, Yee J, Keedy A, et al. Assessment of Bone Mineral Density on CT Colonography. Radiological Society of North America 2008 Scientific Assembly and Annual Meeting; February 18 – February 20 2008, 2008; Chicago IL.
17. Habashy AH, Yan X, Brown JK, et al. Estimation of bone mineral density in children from diagnostic CT images: a comparison of methods with and without an internal calibration standard. *Bone*. 2011;48:1087–1094.
18. Bauer JS, Henning TD, Mueller D, et al. Volumetric quantitative CT of the spine and hip derived from contrast-enhanced MDCT: conversion factors. *AJR Am J Roentgenol*. 2007;188:1294–1301.
19. Baum T, Muller D, Dobritz M, et al. BMD measurements of the spine derived from sagittal reformations of contrast-enhanced MDCT without dedicated software. *Eur J Radiol*. 2011;80:e140–e145.
20. Baum T, Muller D, Dobritz M, et al. Converted lumbar BMD values derived from sagittal reformations of contrast-enhanced MDCT predict incidental osteoporotic vertebral fractures. *Calcif Tissue Int*. 2012;90:481–487.
21. General Assembly of the World Medical A. World Medical Association Declaration of Helsinki: ethical principles for medical research involving human subjects. *J Am Coll Dent*. 2014;81:14–18.
22. Gluer CC, Blake G, Lu Y, et al. Accurate assessment of precision errors: how to measure the reproducibility of bone densitometry techniques. *Osteoporos Int*. 1995;5:262–270.

23. Acu K, Scheel M, Issever AS. Time dependency of bone density estimation from computed tomography with intravenous contrast agent administration. *Osteoporos Int*. 2014;25:535–542.

24. Wilmink JT, Roukema JG, van den Burg W. Effects of i.v. contrast administration on intraspinal and paraspinal tissues: a CT study. 2. Visual assessment. *AJNR Am J Neuroradiol*. 1988;9:191–193.

25. Jorgensen HS, Winther S, Bottcher M, et al. Effect of intravenous contrast on volumetric bone mineral density in patients with chronic kidney disease. *J Clin Densitom*. 2016.

26. Gruber M, Bauer JS, Dobritz M, et al. Bone mineral density measurements of the proximal femur from routine contrast-enhanced MDCT data sets correlate with dual-energy X-ray absorptiometry. *Eur Radiol*. 2013;23:505–512.

27. Ziemlewicz TJ, Maciejewski A, Binkley N, et al. Direct comparison of unenhanced and contrast-enhanced CT for opportunistic proximal femur bone mineral density measurement: implications for osteoporosis screening. *AJR Am J Roentgenol*. 2016;206:694–698.

28. Ziemlewicz TJ, Maciejewski A, Binkley N, et al. Opportunistic quantitative CT bone mineral density measurement at the proximal femur using routine contrast-enhanced scans: direct comparison with DXA in 355 adults. *J Bone Miner Res*. 2016.

29. Lochmüller EM, Eckstein F, Kaiser D, et al. Prediction of vertebral failure loads from spinal and femoral dual-energy X-ray absorptiometry, and calcaneal ultrasound: an in situ analysis with intact soft tissues. *Bone*. 1998;23:417–424.

30. Lochmüller EM, Bürklein D, Kuhn V, et al. Mechanical strength of the thoracolumbar spine in the elderly: prediction from in situ dual-energy X-ray absorptiometry, quantitative computed tomography (QCT), upper and lower limb peripheral QCT, and quantitative ultrasound. *Bone*. 2002; 31:77–84.

31. Alarkawi D, Bliuc D, Nguyen TV. Contribution of Lumbar Spine BMD to Fracture Risk in Individuals With T-Score Discordance. *J Bone Miner Res*. 2016;31:274–280.

32. Hansen KE, Vallarta-Ast N, Krueger D, et al. Use of the lowest vertebral body T-score to diagnose lumbar osteoporosis in men: is "cherry picking" appropriate? *J Clin Densitom*. 2004;7: 376–381.